

# Structure dynamics reveal key residues essential for the sense of 1-dodecanol by *Cydia pomonella* pheromone binding protein 2 (CpomPBP2)

Zhen Tian,<sup>a,b</sup> Yue Li,<sup>a</sup> Tong Zhou,<sup>b</sup> Xuan Ye,<sup>a</sup> Ruichi Li<sup>a</sup> and Jiyuan Liu<sup>a\*</sup> 



## Abstract

**BACKGROUND:** *Cydia pomonella*, a worldwide quarantine fruit pest, causes great damage to fruit production every year. Sex pheromone-mediated control of *C. pomonella* has been widely used. As an indispensable ingredient of commercial sex attractants, 1-dodecanol (Dod) works to synergize the effect of codlemone in attracting male moths of *C. pomonella*. The interactions between Dod and its transporter protein, *C. pomonella* pheromone-binding protein 2 (CpomPBP2), provide inspiration for chemical optimizations to improve the synergistic effects of Dod.

**RESULTS:** In this research, molecular simulations and biological verifications were used in combination to uncover key residues in CpomPBP2 essential for sensing Dod. After performing 150 ns molecular dynamics (MD) simulations, the C1–C12 chain of Dod was found to be locked by the van der Waals energy contributed by the hydrophobic residues Phe12, Leu68, and Ile113, whereas the -OH part of Dod was anchored by the H-bond derived from Glu98 and the salt-bridge derived from Arg109. Because of the importance of these two electrostatic interactions, Glu98 and Arg109 were further verified as key residues in determining the binding affinity between Dod and CpomPBP2. In addition, interactions unfavorable to the binding of Dod were described.

**CONCLUSION:** The research detailed the discovery of key residues involved in CpomPBP2–Dod interactions. Our results provide guidance and caution for the prospective discovery, optimization, and design of novel chemicals with a similar or stronger synergistic effect to codlemone in controlling *C. pomonella*.

Supporting information may be found in the online version of this article.

**Keywords:** *Cydia pomonella*; odorant-binding proteins; pheromone synergist; molecular dynamics; pairwise free-energy decomposition; site-directed mutagenesis

## 1 INTRODUCTION

Codling moth, *Cydia pomonella*, is a major cosmopolitan pest of pome and stone fruits (apple, pear, peach, etc.), causing severe damage to global fruit production.<sup>1,2</sup> Like other Lepidopteran insects, *C. pomonella* relies heavily on chemical signals to regulate its behavior including host finding, mating, and oviposition.<sup>2,3</sup> To date, a large amount of research has been undertaken on the control of pest insects by regulating their behaviors.<sup>4–6</sup>

Currently, the most widely used insect behavior regulators are sex pheromones packaged in slow-release generators.<sup>7–9</sup> For *C. pomonella*, pheromone-mediated management strategies (mating disruption, mass trapping, etc.) have been successfully applied and have shown promising results in commercial orchards.<sup>2,10,11</sup> The sex pheromone of *C. pomonella* is reported to be a multicomponent mixture, with 1-dodecanol (Dod, CAS: 112-53-8) the second-most abundant compound.<sup>12,13</sup> Even though Dod alone has no effects on attracting *C. pomonella*, it aids in orientation and acts as a synergist of codlemone (E,E-8,10-dodecadienol, CAS: 33956-49-9), the main component of

the codling moth sex pheromone.<sup>14,15</sup> As reported, Dod acts by widening the dose range over which male moths of *C. pomonella* are optimally attracted to codlemone.<sup>2,13</sup> Dod and codlemone are used in a blend in current commercial sexual attractants and mating disruptors for *C. pomonella*.<sup>2,15,16</sup>

Sensilla distributed on insect antennae are dominant olfactory organs sensing semiochemicals bearing specific chemical signals.<sup>17,18</sup> In most cases, odorant-binding proteins (OBPs) are thought to be the main proteins responsible for the recognition

\* \*Correspondence to: J Liu, Key Laboratory of Plant Protection Resources & Pest Management of the Ministry of Education, College of Plant Protection, Northwest A&F University, Yangling 712100, Shaanxi, China, E-mail: kingjly0818@hotmail.com

a Key Laboratory of Plant Protection Resources & Pest Management of the Ministry of Education, College of Plant Protection, Northwest A&F University, Yangling, China

b College of Horticulture and Plant Protection, Yangzhou University, Yangzhou, China

and transportation of semiochemicals within the antennal sensilla.<sup>19,20</sup> As an OBP, *C. pomonella* pheromone binding protein 2 (CpomPBP2) is found in the antennae of both sexes.<sup>21</sup> Among the compounds isolated from female glands and apple volatiles, Dod exhibited the highest affinity for CpomPBP2. In addition, CpomPBP2 is superior to other known OBPs from *C. pomonella* in binding with Dod.<sup>21,22</sup> The high affinity between CpomPBP2 and Dod indicates that CpomPBP2 may function to transport Dod across the sensillum lymph to odorant receptors (ORs) located on the membranes of olfactory neurons.

As a known synergist to codlemone in attracting *C. pomonella*, Dod enhances male attraction at low codlemone doses. But how Dod binds to its transporter CpomPBP2 and what residues are involved in the binding process remain unknown. To clarify these questions, a complex model formed by CpomPBP2 and Dod was initially subjected to 150 ns molecular dynamics (MD) simulations. After determining the MD representative conformation of the CpomPBP2–Dod complex, binding free-energy calculations, pairwise per-residue free-energy decomposition, site-directed mutagenesis, and a competitive binding assay were used in combination to determine the residues essential for sensing of Dod by CpomPBP2. During analysis, interactions unfavorable to the binding of Dod to CpomPBP2 were also highlighted, giving opportunities for active enhancement of Dod. Our results have great significance for the prospective discovery of novel chemicals with functions similar to Dod in enhancing the male-attraction effect of codlemone, and in boosting the development and widespread use of pheromone-mediated management to control *C. pomonella*.

## 2 MATERIALS AND METHODS

### 2.1 MD simulations

A 3D model of the CpomPBP2–Dod complex (Fig. S1) constructed in our previous research was subjected to the Amber12 package for 150 ns MD simulations.<sup>21,23,24</sup> To prepare for MD simulations, the CpomPBP2–Dod model was immersed in a rectangular box of explicit transferable intermolecular potential with 3 points (TIP3P) water with a minimum solute wall distance of 8 Å.<sup>25</sup> Na<sup>+</sup> ions were added to keep the entire system neutral.<sup>26</sup> The parameters and charge of the Dod ligand were optimized using General Amber Force Field (GAFF) and AM1-BCC (semi-empirical (AM1) with bond charge correction (BCC)) methods, and counterparts for the protein CpomPBP2 were set using ff9SB.<sup>27–29</sup> To remove possible unfavorable contacts, the free-energy of the CpomPBP2–Dod complex was minimized through successive application of the steepest descent method (5000 steps) and conjugate gradient method (5000 steps). MD simulations of the CpomPBP2–Dod complex were performed in Amber12 without restraint. During the equilibration phase of MD simulations, the prepared complex was heated to 300 K in 500 ps in the NVT ensemble (canonical ensemble) and kept at 300 K for 5 ns under constant pressure for unstrained equilibration. To prevent an abrupt jump in potential energy, the same conditions as in the equilibration phase were adopted in the production phase. Throughout MD simulations, coordinates were recorded every 10 ps; this helps to keep the conformations uncorrelated. The isothermal isobaric ensemble (NPT) used in the equilibration and production phases was realized by a Berendsen barostat.<sup>30</sup> MD trajectories produced in the 150 ns were analyzed using the AmberTools13 package.<sup>23</sup>

### 2.2 Binding free-energy calculation

According to our previous research, the molecular mechanics Poisson–Boltzmann surface area (MM-PBSA) method is rational enough to calculate the theoretical binding free-energy ( $\Delta G_{\text{bind-cal}}$ ).<sup>24,31,32,33</sup> Thus the MM-PBSA method in Amber12 software was adopted to estimate  $\Delta G_{\text{bind-cal}}$  of the CpomPBP2–Dod complex.<sup>31,34,35</sup> The MM-PBSA method calculates trajectory averages based mainly on force field energies combined with Poisson–Boltzmann electrostatics and surface area terms.<sup>36,37</sup> In the MM-PBSA method, the  $\Delta G_{\text{bind-cal}}$  of CpomPBP2–Dod binding was obtained from the difference between the free-energy of the CpomPBP2–Dod complex ( $\Delta G_{\text{complex}}$ ) and unbound CpomPBP2 ( $\Delta G_{\text{protein}}$ ) and Dod ( $\Delta G_{\text{ligand}}$ ), as shown in Eqn (1).<sup>31</sup>

$$\Delta G_{\text{bind-cal}} = \Delta G_{\text{complex}} - (\Delta G_{\text{protein}} + \Delta G_{\text{ligand}}) \quad (1)$$

For the CpomPBP2–Dod complex, we calculated  $\Delta G_{\text{bind-cal}}$  values for the 15 000 snapshots of the MD trajectories (one snapshot for each 10 ps during the 150 ns MD simulations). The final  $\Delta G_{\text{bind-cal}}$  was the average of calculated  $\Delta G_{\text{bind-cal}}$  values for these snapshots.

### 2.3 Pairwise per-residue free-energy decomposition

Definition of the CpomPBP2–Dod interaction energy spectra is needed to detail interactions between CpomPBP2 and Dod. Based on the MD representative conformation of the CpomPBP2–Dod complex, energy spectra of the CpomPBP2–12:OH interface were depicted by pairwise per-residue free-energy decomposition.<sup>38–40</sup> In the current research, pairwise per-residue free-energy decomposition was performed using the MM-PBSA method from the mmpbsa.py module of AmberTools13.<sup>41,42</sup> The whole process was modified from our former research.<sup>43</sup>

### 2.4 Site-directed mutagenesis

Residue sites for site-directed mutagenesis were selected based on the comprehensive results of pairwise assays performed above and computational alanine scanning in our previous research.<sup>21</sup> Site-directed mutation of CpomPBP2 was implemented following the instruction manual (Vazyme, China). Briefly, the wild-type CpomPBP2 gene was subcloned into PMD-19T vector to generate the *PMD19T–CpomPBP2* plasmid. Primers for site-directed mutagenesis were prepared accordingly (Vazyme). These primers (Table S1) were used to perform polymerase chain reactions (PCR) with *PMD19T–CpomPBP2* plasmids as a template. After removing the templates by DpnI digestion (37 °C, 90 min), PCR products were treated with Exnase II (37 °C, 30 min) to promote cyclization. Reaction products were transformed into DH5 $\alpha$ -competent cells, coated plates, and a select monoclonal colony. Mutant CpomPBP2 genes were verified by gene sequencing (Tsingke, China).

### 2.5 Protein expression and purification

To obtain recombinant wild-type CpomPBP2 (CpomPBP2WT) protein, pCold III (TaKaRa, Japan) was selected as the protein expression vector and TransB (DE3) strain (Transgen, China) was taken as the host cell. After transformation, the host containing pColdIII–CpomPBP2 plasmids was cultured at 37 °C, 200 rpm. When the optical density at 600 nm (OD<sub>600</sub>) reached 0.6, the cultured strain was precooled to 15 °C before addition of isopropyl  $\beta$ -D-thiogalactopyranoside (IPTG; 0.6 mM). Thereafter, the strain was cultured for 24 h at 15 °C and 160 rpm to induce expression

of CpomPBP2WT. The cultured strain was collected (5000 rpm, 10 min), sonicated (10 s work/10 s stop for 10 min), and centrifuged (12 000 g, 30 min). The resultant supernatants were loaded onto a Ni<sup>2+</sup>-NTA resin column (Qiagen, Germany) for protein purification. Recombinant CpomPBP2 protein equipped with a His tag was eluted using 300 mM imidazole. After 15% sodium dodecyl sulfate–polyacrylamide gel electrophoresis (SDS–PAGE), fractions containing CpomPBP2 protein were pooled. His-tag cleavage was achieved by incubating with PreScission protease (GE Healthcare) at 4 °C for 12 h, followed by a re-purification step using a Ni<sup>2+</sup>-NTA resin column (Qiagen) to remove the His tag and PreScission protease. Finally, the purified sample was checked by 15% SDS–PAGE, dialyzed against 10 mM phosphate-buffered saline (PBS; pH 7.4), and quantified using a Bradford kit (Solarbio, China). Purified CpomPBP2 protein was kept at –80 °C for further tests. Expression and purification of mutant CpomPBP2 (CpomPBP2MT) proteins were performed similarly.<sup>26</sup>

## 2.6 Competitive binding assay

With N-phenyl-1-naphthylamine (1-NPN) as the fluorescent probe, a competitive binding assay was used to measure changes in affinity between Dod and recombinant CpomPBP2 proteins (CpomPBP2WT and CpomPBP2MT).<sup>24,32,44</sup> Briefly, the dissociation constants between 1-NPN and recombinant CpomPBP2 proteins were determined by titrating 2 μM protein solutions with 1 mM 1-NPN (final concentration: 0.5–20 μM). To test the binding affinity between Dod and CpomPBP2WT/CpomPBP2MT proteins, 10 mM PBS (pH 7.4) solutions containing 2 μM recombinant CpomPBP2 proteins and 2 μM 1-NPN were titrated against 1 mM Dod (final concentration: 0–64 μM) in three replications. Fluorescence responses were detected using a Hitachi F-2700 spectrofluorometer (Hitachi, Japan), with an excitation wavelength of 337 nm and emission spectra were recorded between 350 and 500 nm.

## 2.7 Statistics

GraphPad Prism 6.0 (GraphPad Software, Inc., California, USA) was used to analyze the competitive binding assay data. Dissociation constants ( $K_d$ ) between recombinant CpomPBP2 proteins and Dod were calculated using Eqn (2).<sup>22,24</sup>

$$K_d = IC_{50} / (1 + [1-NPN] / K_{1-NPN}) \quad (2)$$

In Eqn (2),  $IC_{50}$  is the concentration of Dod quenching the fluorescence intensity by half;  $[1-NPN]$  is the free concentration of 1-NPN;  $K_{1-NPN}$  is the  $K_d$  between CpomPBP2 protein and 1-NPN.

The experimental binding free-energy ( $\Delta G_{bind-exp}$ ) for the complex formed by Dod and wild-type CpomPBP2 was calculated using Eqn (3).<sup>24,32</sup>

$$\Delta G_{bind-exp} = RT \ln K_{d-WT} \quad (3)$$

In Eqn (2),  $R$  and  $T$  are the ideal gas constant and temperature in Kelvin, respectively.  $K_{d-WT}$  is the  $K_d$  value between wild-type CpomPBP2 protein and Dod.

Changes in the experimental binding free-energy ( $\Delta \Delta G_{bind-exp}$ ) caused by mutation of target residues were calculated based on corresponding  $K_d$  values using Eqn (4).<sup>24,43</sup>

$$\Delta \Delta G_{bind-exp} = RT \ln (K_{d-MT} / K_{d-WT}) \quad (4)$$

In Eqn (4),  $R$  is the ideal gas constant,  $T$  is the temperature in Kelvin,  $K_{d-MT}$  is the  $K_d$  value between mutant CpomPBP2 proteins and

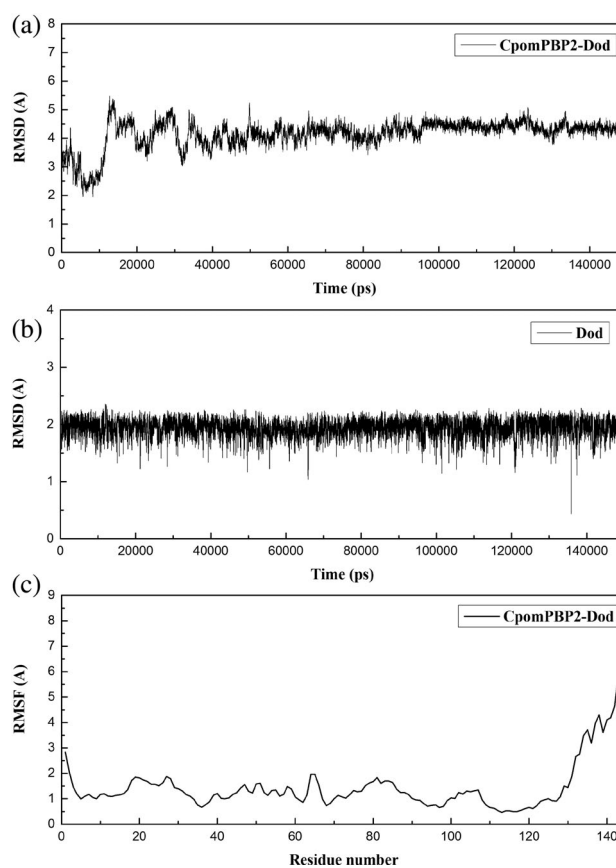


**Figure 1** Molecular dynamics (MD) simulations of the CpomPBP2–Dod complex. (A) Root mean square deviation (RMSD) values for the CpomPBP2–Dod complex in the process of 150 ns MD simulations. (B) RMSD values for the ligand Dod in the process of 150 ns MD simulations. (C) Root mean square fluctuations for each residue derived from the CpomPBP2–Dod complex in the process of 150 ns MD simulations. Dod, 1-dodecanol; CpomPBP2–Dod, CpomPBP2–Dod complex.

Dod,  $K_{d-WT}$  is the  $K_d$  value between wild-type CpomPBP2 proteins and Dod.

## 3 RESULTS

### 3.1 The CpomPBP2–Dod complex is stable during MD simulations

The CpomPBP2–Dod complex (Fig. S1A) constructed in our former research was subjected to 150 ns MD simulations.<sup>21</sup> As shown in Fig. 1(A), the CpomPBP2–Dod complex reached equilibrium at ~50 ns, and its averaged root-mean-square deviation (RMSD) fluctuated around 4.30 Å (SD = 0.22 Å). Specifically for the ligand Dod in the CpomPBP2–Dod system, equilibrium was achieved immediately after initiation of the 150 ns MD simulations with an RMSD of  $1.93 \pm 0.15$  Å (Fig. 1B). Equilibrium in the CpomPBP2–Dod system indicated the stability and rationality of the complex formed by CpomPBP2 and Dod.

To obtain further information on the structure of the CpomPBP2–Dod complex, root-mean-square fluctuation (RMSF) analysis was carried out to reveal its flexibility and local motion characteristics (Fig. 1C). As previously reported,<sup>21</sup> the 3D model of CpomPBP2 contained two secondary structure elements, namely  $\alpha$ -helices and free loops (Fig. S1A). Considering the results in Figs 1(C) and S1, it is easy to show that  $\alpha$ -helices were more rigid

than loops, which was particularly evident in the N-terminus and C-terminal tail. It should be noted that, due to their large distance from the binding pocket of CpomPBP2, the dramatic flexibility of the N- and C-termini has no apparent effect on the interaction contacts of the CpomPBP2–Dod complex, further suggesting stability of the complex formed by CpomPBP2 and Dod.

### 3.2 Binding mode analysis of the CpomPBP2–Dod complex

An average-linkage algorithm and pairwise RMS were applied in conjunction to cluster the MD trajectories produced during the 150 ns MD simulations. As shown in Table S2 and Fig. S2, five clusters were obtained, with Cluster I and Cluster II having the highest rates of 44% and 30.4%, respectively. It is interesting that Dod possessed similar binding modes in the representative conformations of the two dominant clusters. As shown in Fig. S3, the alkyl group of Dod was located in the hydrophobic pocket composed of residues including by Phe12, Leu68 and Ile113. By contrast, the hydroxyl group (-OH) was found to interact with hydrophilic residues including Glu98 and Arg109. Specifically, the O1 atom from -OH of Dod formed an H-bond interaction with the OE atom of the Glu98 side-chain. A salt-bridge interaction was detected between -OH of Dod and the side-chain of Arg109. Tiny differences between the binding modes of Dod in the representative conformations of Cluster I and Cluster II also exist. Taking the H-bond as an example, the distance of O–O atoms forming the H-bond changed from 1.9 Å in Cluster II to 1.7 Å in Cluster I (Fig. S3). Considering the higher occupation rate and stronger H-bond interaction, the conformation derived from Cluster I was closer to the representative conformation extracted from the 150 ns MD trajectories (Fig. 2).

### 3.3 Theoretical binding free-energy calculation

Based on the MD representative conformation (Fig. 2), theoretical binding free-energy ( $\Delta G_{\text{bind-cal}}$ ) of the CpomPBP2–Dod complex was calculated using the MM-PBSA method.<sup>31,36,37,45,46</sup> As revealed by the free-energy items listed in Table 1, van der Waals interactions ( $\Delta E_{\text{vdw}} = -34.83 \text{ kcal mol}^{-1}$ ) were the most dominant forces driving formation and maintenance of the CpomPBP2–Dod complex. Considering the strong salt bridge (between Arg109 and -OH of Dod) and the H-bond (between Glu98 and -OH of Dod) in the CpomPBP2–Dod system, the free-energy contribution derived from electrostatic interactions ( $\Delta E_{\text{ELE}}$ ) was fairly evident, with a value of  $-7.78 \text{ kcal mol}^{-1}$ . In

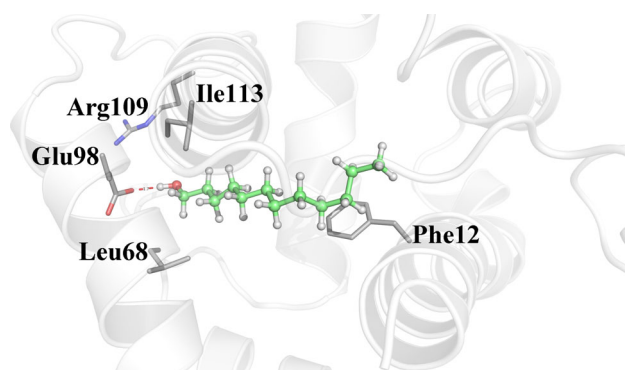


**Figure 2** Representative conformation of the CpomPBP2–Dod complex produced based on the molecular dynamics trajectories. Representative residues Phe12, Leu68, Glu98, Arg109, and Ile113, are marked on the binding interface. The ligand Dod is shown as a sphere–stick model.

the representative conformation of the CpomPBP2–Dod complex, the nonpolar contribution to the solvation free-energy ( $\Delta E_{\text{SURF}}$ ) was also favorable for binding of Dod to CpomPBP2. According to the results of an empirical model,  $\Delta E_{\text{SURF}}$  of the CpomPBP2–Dod complex was estimated to be as high as  $-28.53 \text{ kcal mol}^{-1}$ . However, free-energies unfavorable for the CpomPBP2–Dod interaction were also detected. For example, unfavorable energy from the polar part of solvation free-energy ( $\Delta E_{\text{EPB}}$ ) reached up to  $13.84 \text{ kcal mol}^{-1}$ . The SEM of each free-energy item was limited to  $0.40 \text{ kcal mol}^{-1}$  (Table 1), indicating the high accuracy of the theoretical binding free-energy calculated using the MM-PBSA method.

### 3.4 Pairwise per-residue free-energy decomposition

Based on the MD representative conformation of the CpomPBP2–Dod complex, the pairwise energy contribution ( $\Delta E_{\text{pair}}$ ) of each residue was estimated using pairwise per-residue free-energy decomposition. It is clear in Fig. 3(A) that five residues (Phe12, Leu68, Glu98, Arg109, and Ile113) made relatively significant  $\Delta E_{\text{pair}}$  contributions ( $\geq -2.00 \text{ kcal mol}^{-1}$ ) compared with other residues, so the pairwise energy contributions between these five residues and Dod were selectively analyzed (Fig. 3B). As shown in Fig. 3(B) and Table 2, Glu98 and Arg109 contributed the highest  $\Delta E_{\text{pair}}$ , with values of  $-4.17$  and  $-3.95 \text{ kcal mol}^{-1}$ , respectively. Table 2 shows that the  $\Delta E_{\text{pair}}$  of Glu98 and Arg109 was predominantly derived from their remarkable electrostatic energy contributions ( $-6.87 \text{ kcal mol}^{-1}$  for Glu98,  $-3.28 \text{ kcal mol}^{-1}$  for Arg109). Such high electrostatic energy contributions are in line with H-bond and salt-bridge interactions formed between -OH of Dod and Glu98/Arg109. For Glu98, it should not be ignored that a high polar solvation energy ( $2.27 \text{ kcal mol}^{-1}$ ) unfavorable to the binding of Dod was detected, even though its contribution to the total  $\Delta E_{\text{pair}}$  was remarkable (Table 2). Unfavorable van der Waals interactions derived from Glu98 and Arg109 were detected also. For Glu98 in particular, the unfavorable van der Waals energy was close to  $1.00 \text{ kcal mol}^{-1}$  (Table 2).

In addition to Glu98 and Arg109, three other hydrophobic residues (Phe12, Leu68, and Ile113) showed a superior pairwise energy contribution, with  $\Delta E_{\text{pair}}$  ranging from  $-2.00$  to  $-3.00 \text{ kcal mol}^{-1}$ . For Phe12 in particular,  $\Delta E_{\text{pair}}$  was as high as  $-2.90 \text{ kcal mol}^{-1}$ . For the three residues, the van der Waals and nonpolar solvation energy contributions were all significant ( $> -1.00 \text{ kcal mol}^{-1}$ ) and favorable for binding of Dod to CpomPBP2. Specifically, the favorable van der Waals energy ( $-1.65 \text{ kcal mol}^{-1}$ ) provided by Phe12 was due to hydrophobic contact between Phe12 and the C1–C6 part of the Dod alkyl group (Figs 3B and S4). The large contributions of Ile113 ( $-1.28 \text{ kcal mol}^{-1}$ ) and Leu68 ( $-1.22 \text{ kcal mol}^{-1}$ ) to van der Waals forces can be attributed to their hydrophobic interactions with the C7–C9 and C10–C12 regions of Dod, respectively (Table 2, Figs 3B and S4). Notably, the electrostatic energy ( $-0.049 \text{ kcal mol}^{-1}$ ) and polar solvation energy ( $-0.21 \text{ kcal mol}^{-1}$ ) derived from Ile113 were both weak but favorable for binding of Dod to CpomPBP2. The introduction of polar and charged groups like hydroxyl (-OH) to the C9 site of Dod would be feasible to boost the binding affinity between CpomPBP2 and Dod (Fig. S4).

### 3.5 Site-directed mutagenesis and protein expression

After comprehensive consideration of the results produced by pairwise free-energy decomposition and computational alanine scanning (reported in our previous research),<sup>21</sup> four residues, Phe12, Glu98, Arg109 and Ile113, were selected for

**Table 1** Theoretical and experimental binding free-energy<sup>a</sup> for the binding of Dod to wild-type CpomPBP2 protein

Contribution	$\Delta E_{\text{ele}}$	$\Delta E_{\text{vdW}}$	$\Delta E_{\text{EPB}}$	$\Delta E_{\text{ESURF}}$	$\Delta G_{\text{gas}}$	$\Delta G_{\text{sol}}$	$\Delta G_{\text{bind-cal}}^b$	$\Delta G_{\text{bind-exp}}^c$
CpomPBP2WT <sup>d</sup>	-7.78 (0.19)	-34.83 (0.21)	13.84 (0.27)	-28.53 (0.06)	-42.61 (0.21)	31.33 (0.34)	-11.27 (0.40)	-9.57 (0.28)

<sup>a</sup>All values are shown in kcal mol<sup>-1</sup> with corresponding SEM in parentheses.

<sup>b</sup> $\Delta G_{\text{bind-cal}}$  is the theoretical binding free-energy of the CpomPBP2–Dod complex.

<sup>c</sup> $\Delta G_{\text{bind-exp}}$  is the experimental binding free-energy of the CpomPBP2–Dod complex.

<sup>d</sup>CpomPBP2WT is the wild-type CpomPBP2 protein.

site-directed mutagenesis. Wild-type and mutant CpomPBP2 genes were cloned into pCold III vectors and expressed in TransB (DE3) strains. It should be noted that pCold III replaced

pet-28a(+) used in our previous report. As a cold shock plasmid, pCold III could promote the soluble expression of target proteins at low temperatures. Meanwhile, TransB (DE3) strains aid formation of disulfide bonds which are important for the correct folding of CpomPBP2. Because of the double effects of vector and host strain, soluble expression of wild-type and mutant CpomPBP2 proteins was successfully realized (Figs S5 and S6). For convenience, wild-type CpomPBP2 protein was abbreviated as CpomPBP2WT, CpomPBP2 proteins mutated at the sites of Phe12, Glu98, Arg109, and Ile113 were named CpomPBP2F12A, CpomPBP2E98A, CpomPBP2R109A, and CpomPBP2I113A.

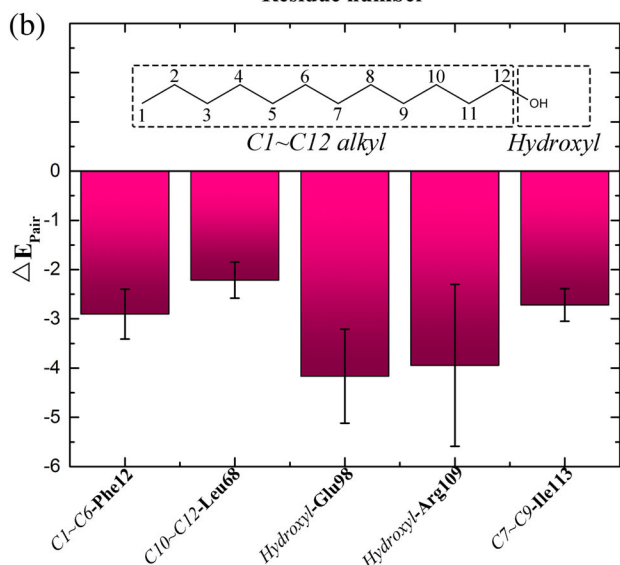
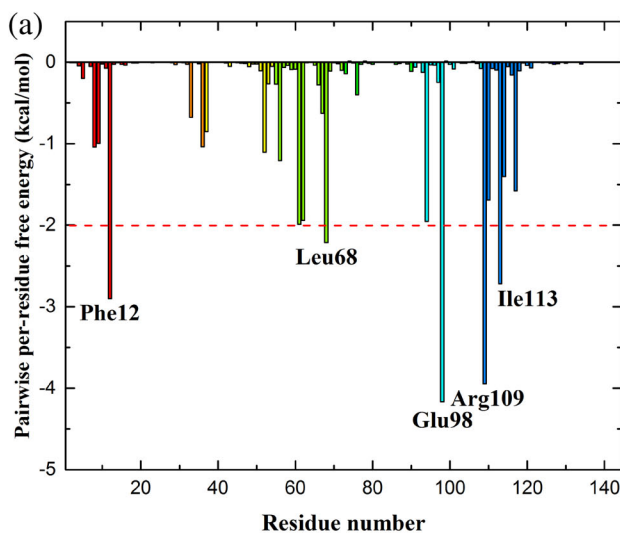


**Figure 3** Pairwise per-residue free-energy decomposition of the CpomPBP2–Dod complex. (A) Energy spectra presenting the energy contribution of each residue in the CpomPBP2–Dod complex. Five residues (Phe12, Leu68, Glu98, Arg109, and Ile113) contribute beyond  $-2.00$  kcal mol<sup>-1</sup> free-energy. (B) Energy spectra presenting the interactions formed between representative residues and groups of Dod. C1–C12 chain of Dod mainly interacts with hydrophobic residues represented by Phe12, Leu68, and Ile113. The hydroxyl group of Dod mainly forms electrostatic interactions with Glu98 and Arg109.

### 3.6 Calculating experimental binding free-energy

The experimental binding free-energy ( $\Delta G_{\text{bind-exp}}$ ) of the CpomPBP2–Dod complex was calculated using the  $K_d$  value between wild-type CpomPBP2 protein and Dod ( $K_{d-WT}$ ). Using a competitive binding assay,  $K_{d-WT}$  was determined as  $0.18 \pm 0.09 \mu\text{M}$  (Fig. 4A), giving a  $\Delta G_{\text{bind-exp}}$  for the CpomPBP2–Dod complex of  $-9.57$  kcal mol<sup>-1</sup> (Table 1). The value of  $\Delta G_{\text{bind-exp}}$  was in qualitative agreement with  $\Delta G_{\text{bind-cal}}$  ( $-11.27$  kcal mol<sup>-1</sup>) calculated using the MM-PBSA method, and the difference was within acceptable limits ( $2.00$  kcal mol<sup>-1</sup>). The consistency of  $\Delta G_{\text{bind-exp}}$  and  $\Delta G_{\text{bind-cal}}$  further indicated the stability and rationality of the complex formed by CpomPBP2 and Dod.

### 3.7 Hot-spot determination

Before evaluating changes in the binding affinity caused by site-directed mutation,  $K_d$  values between the fluorescent probe 1-NPN and wild-type/mutant CpomPBP2 proteins, namely  $K_{1-NPN}$ , were determined and compared. As expected, individual replacement of Phe12, Glu98, Arg109, and Ile113 by Ala had no significant effect on the binding of 1-NPN to CpomPBP2 proteins (Fig. S6). Consequently, for convenience, the  $K_{1-NPN}$  value of wild-type CpomPBP2 protein was taken as the sole  $K_{1-NPN}$  in subsequent competitive binding assays. As shown in Fig. 4, individual mutation of Phe12, Glu98, Arg109, and Ile113 into Ala was unfavorable for the binding of Dod. Of the four mutant CpomPBP2 proteins, CpomPBP2E98A and CpomPBP2R109A showed minimum affinity to Dod, with  $K_d$  values of  $135.97 \pm 9.56$  and  $147.15 \pm 6.91 \mu\text{M}$ , respectively. The  $K_d$  values for CpomPBP2E98A and CpomPBP2R109A were further transformed into changes in the experimental binding free-energy ( $\Delta\Delta G_{\text{bind-exp}}$ ) using Eqn (3) (Table 2). According to the thresholds for hot-spots ( $\Delta\Delta G_{\text{bind}} \geq 4.00$  kcal mol<sup>-1</sup>), warm spots ( $2.00$  kcal mol<sup>-1</sup>  $\leq \Delta\Delta G_{\text{bind}} < 4.00$  kcal mol<sup>-1</sup>), and null spots ( $\Delta\Delta G_{\text{bind}} < 2.00$  kcal mol<sup>-1</sup>) provided by Moreira *et al.*,<sup>47</sup> Glu98 ( $\Delta\Delta G_{\text{bind-exp}} = 4.08$  kcal mol<sup>-1</sup>) and Arg109 ( $\Delta\Delta G_{\text{bind-exp}} = 4.13$  kcal mol<sup>-1</sup>) were classified as hot-spots (Table 3), suggesting they have key roles in the binding of Dod to CpomPBP2 proteins. The key roles

**Table 2** Decomposition of binding free-energy on a pairwise per-residue level<sup>a</sup>

Dod - Residue	van der Waals	Electrostatic	Polar solvation	Non-polar solvation	Total
Phe12	-1.65	0.014	0.16	-1.42	-2.90 ± 0.51
Leu68	-1.22	0.40	-0.34	-1.06	-2.22 ± 0.37
Glu98	0.80	-6.87	2.27	-0.36	-4.17 ± 0.96
Arg109	0.19	-3.28	-0.32	-0.54	-3.95 ± 1.64
Ile113	-1.28	-0.049	-0.21	-1.18	-2.72 ± 0.33

<sup>a</sup>Energies are shown as contributions from van der Waals energy, electrostatic energy, polar solvation energy, non-polar solvation and their sum for the CpomPBP2–Dod complex. All values are given in kcal mol<sup>-1</sup>.

of Glu98 and Arg109 in determining the affinity between Dod and CpomPBP2 protein can be attributed to their strong electrostatic interactions with -OH of Dod (Figs 2 and S4, Table 2). On mutation of Glu98 and Arg109 to Ala, the salt-bridge derived from Arg109 and the H-bond derived from Glu98, which work to anchor the -OH of Dod, were disrupted, resulting in the low binding ability of CpomPBP2E98A and CpomPBP2R109A to Dod (Fig. 4). Mutation of Phe12 and Ile113 to Ala had a much weaker negative effect on the binding ability of CpomPBP2. From Table 2, it is evident that the  $\Delta\Delta G_{\text{bind-exp}}$  values corresponding to CpomPBP2F12A and CpomPBP2I113A fell within the warm spot range (Table 3), suggesting that hydrophobic interactions provided by side-chains of Phe12 and Ile113 were not strong enough to make them key residues in determining the binding ability of CpomPBP2 protein.

## 4 DISCUSSION

Even though pheromone-mediated management is thought of as an eco-friendly method of controlling *C. pomonella*, it is more commonly used as a supplement to chemical control.<sup>48</sup> Application of pheromone synergists to improve the activity of pheromone lures is feasible and effective. In fact, application of synergists in commercial pheromone lures is fairly common. In *Grapholita molesta* sex attractants containing three active ingredients (E8-dodecenyl acetate, Z8-dodecenyl acetate and Z8-dodecenol), Z8-dodecenol is works as a synergist.<sup>49</sup> However, as an auxiliary material in insect attractants, the presence of pheromone synergists and research into their roles are easily ignored. Currently, data on pheromone synergists are quite limited. Yang et al. reported that racemic linalool, E-farnesene, and Z3-hexenol could synergize a response to codlemone in *C. pomonella*. Noticeably, the synergistic effects of these three compounds were not inferior to that of Dod.<sup>50</sup> However, no further reports are available. Taking Dod as a representative molecule of codlemone synergists,

**Table 3** Experimental binding free-energy changes of the CpomPBP2–Dod complex caused by site-directed mutagenesis

Protein <sup>a</sup>	Cpom PBP2F12A	Cpom PBP2E98A	Cpom PBP2R109A	Cpom PBP2I113A
$\Delta\Delta G_{\text{bind-exp}}$ <sup>b</sup>	2.91	4.08	4.13	3.26

<sup>a</sup>CpomPBP2F12A, CpomPBP2 E98A, CpomPBP2R109A, and CpomPBP2I113A are CpomPBP2 proteins mutated into Ala at the residue sites of Phe12, Glu98, Arg109, and Ile113 respectively.

<sup>b</sup> $\Delta\Delta G_{\text{bind-exp}}$  is the experimental binding free-energy change, all values are shown in kcal mol<sup>-1</sup>.

our research aims to provide suggestions for the prospective discovery of novel synergists with function similar to or stronger than Dod by revealing details of the interaction between CpomPBP2 and Dod.

Using 150 ns MD simulations, a stable conformation close to the actual structure of the CpomPBP2–Dod complex was obtained. Acquisition of a reliable conformation is of great significance for subsequent experiments, including binding mode analysis, binding free-energy calculation, free-energy decomposition, and hot-spot determination. As in other research on the structure of insect OBPs,<sup>26,51,52</sup> van der Waals ( $\Delta E_{\text{vdW}}$ ) and electrostatic energy ( $\Delta E_{\text{ELE}}$ ) were two dominant driving forces in the formation and maintenance of the CpomPBP2–Dod complex. As shown in Table 1,  $\Delta E_{\text{vdW}}$  and  $\Delta E_{\text{ELE}}$  values were as high as -34.83 and -7.78 kcal mol<sup>-1</sup>, respectively. Through further pairwise free-energy decomposition (Fig. 3, Table 2), it can be determined that Phe12, Leu68, Glu98, Arg109, and Ile113 were the top five residues in terms of pairwise free-energy contribution, with hydrophobic residues (Phe12, Leu68, and Ile113) being top donors of van der Waals energy, and hydrophilic residues (Glu98 and Arg109) being dominant providers of electrostatic energy. Considering above results, it could be deduced that the long carbon chain (C1–C12) of Dod is reinforced by hydrophobic contacts derived from hydrophobic residues represented by Phe12, Leu68, and Ile113. As for the -OH in Dod, it is generally anchored by the H-bond and salt-bridge interactions provided by Glu98 and Arg109, respectively. Similar phenomena were also found in interactions between other alcohol pheromones and their corresponding pheromone binding proteins (PBPs). Take the pheromone bombykol from *Bombyx mori* for example, the 16-carbon alcohol is bound in the BmorPBP (PBP from *B. mori*) cavity through numerous hydrophobic interactions and a hydrogen bond formed between -OH and Ser56.<sup>51</sup>

Even though the value of  $\Delta E_{\text{vdW}}$  was much higher than  $\Delta E_{\text{ELE}}$  in the CpomPBP2–Dod complex (Table 1), two residues (Glu98 and Arg109) forming electrostatic interactions with -OH of Dod, rather than hydrophobic residues (Phe12, Leu68, and Ile113), were verified as key residues in determining the binding ability of CpomPBP2. Confirmation of Glu98 as a hot-spot supports the assumption that residues forming H-bond with ligands are usually crucial to the protein–ligand interactions.<sup>24,32,51</sup> As a matter of experience, in protein–ligand interactions involved with insect OBPs, key residues are usually those forming either H-bond or hydrophobic interactions with ligand groups.<sup>26,32,44,53</sup> However, Arg109 providing a salt-bridge interaction, a form of electrostatic interaction rarely described in protein–ligand interactions involved with insect OBPs, was determined as a second key residue for the CpomPBP2–Dod complex.

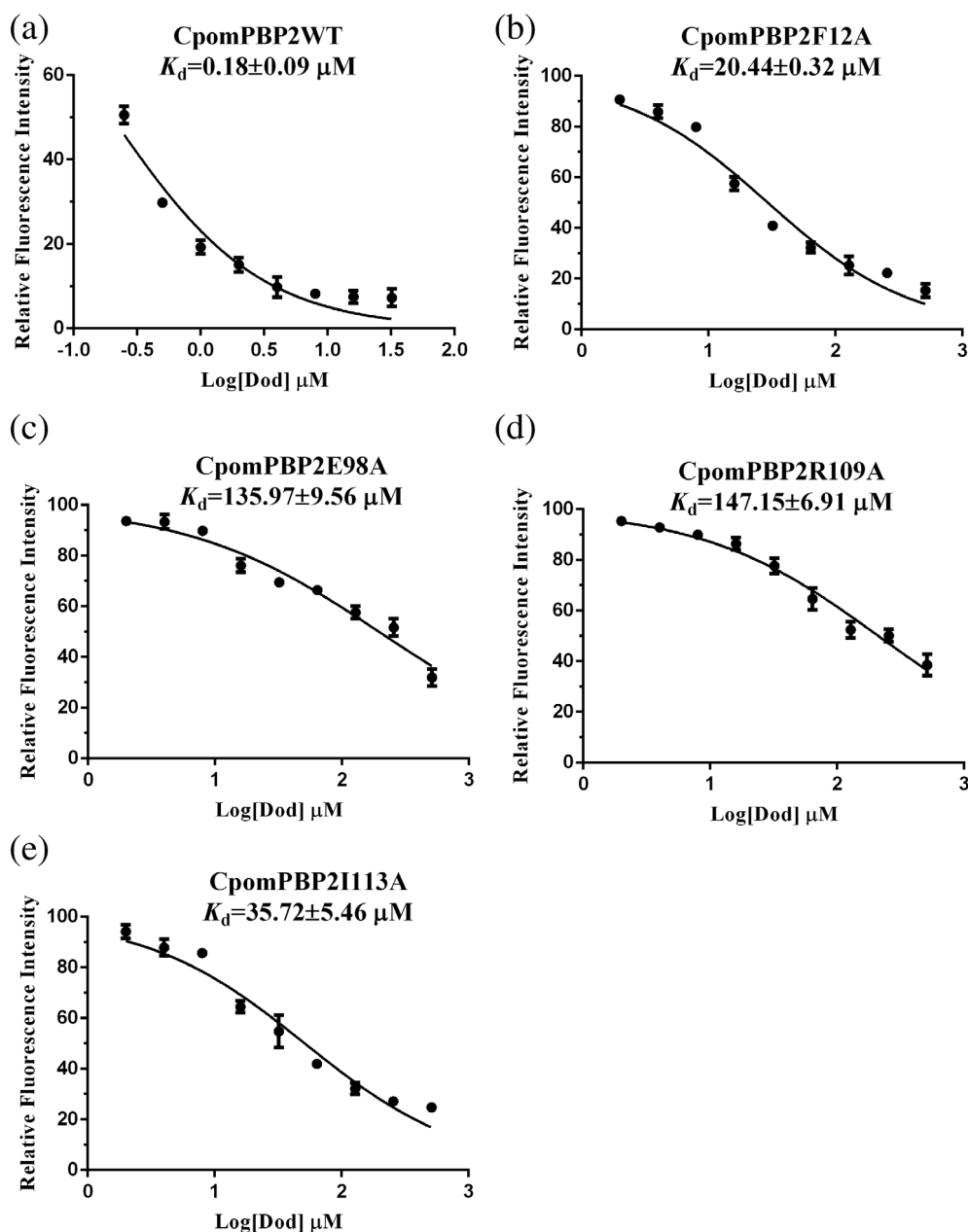


**Figure 4** Binding curves of 1-dodecanol to wild-type (A) and mutant (B) CpomPBP2 proteins. CpomPBP2WT, wild-type CpomPBP2 protein; CpomPBP2F12A, CpomPBP2 E98A, CpomPBP2R109A, and CpomPBP2I113A are CpomPBP2 proteins mutated into Ala at the residue sites of Phe12, Glu98, Arg109, and Ile113 respectively.

In addition to the favorable interactions mentioned above, interactions unfavorable to the binding of Dod to CpomPBP2 were also discussed. In drug discovery, replacing the unfavorable structural parts of prototype molecules with favorable groups is well-established and widely used technique, even though related techniques remain unusual in the field of agriculture. In a report on the development of anti-tubercular drugs, Liu *et al.* found that introducing H-bond acceptors into the benzothiazole ring of TCA1 may lead to the generation of new H-bonds and decrease unfavorable interactions. In fact, the inhibitory effects of TCA1 were improved eightfold when nitrogen was introduced into the C4 position of the TCA1 benzothiazole ring.<sup>54</sup>

Based on accumulated experiences in drug discovery, the existence of unfavorable interactions provides opportunities for the discovery and design of novel chemicals with stronger synergistic

effects than codlemone. For example, the unfavorable polar solvation energy derived from Glu98 reached  $2.27 \text{ kcal mol}^{-1}$  (Table 2), so in the prospective chemical optimization of Dod, groups loaded to Dod should be selected from those unable to generate polar solvation interactions with Glu98. Introducing a nonpolar group into the hydroxyl oxygen of the Dod molecule is recommended. Moreover, the unfavorable van der Waals energy contributed by Glu98 and Arg109 was also remarkable (Table 2). As shown in Fig. S4, C12 derived from the backbone of Dod was spatially close to the side-chains of Glu98 and Arg109. Therefore, actions to load hydrophilic groups onto the site (C12) of Dod may enhance the CpomPBP2–Dod interaction. Unfavorable electrostatic and polar solvation energies derived from Phe12 were small, but did exist. The affinity between CpomPBP2 and Dod would benefit from the presence of polar groups with the C3 or

C4 of Dod located around the phenyl group of the Phe12 side-chain. Unfavorable energy was also derived from electrostatic interactions between Leu68 and the C10–C12 part of Dod (Table 2). Uncharged and nonpolar groups are advised for the C10–C12 sites when optimizing Dod as avoidance of electrostatic interactions with the Leu68 side-chain helps promote the binding affinity between Dod and CpomPBP2.

Finally, it should be noted that the value of  $K_{d-WT}$  obtained in this research was more than ten times lower than reported previously.<sup>21</sup> The increase in binding ability of recombinant CpomPBP2 protein can be attributed to improvements in the adopted prokaryotic expression system. As mentioned above, the host strain (TransB) and expression vector (pCold III) act to promote the yield and quality of soluble CpomPBP2 protein. Moreover, after removing the His tag, the two amino acids (Gly and Pro) attached to the N-terminus of recombinant CpomPBP2 protein have little effect on the binding ability of CpomPBP2, especially considering that the N-terminus of CpomPBP2 is far from the binding cavity.<sup>21</sup> The improved quality of the recombinant CpomPBP2 protein contributed to the higher binding affinity to Dod in this research.

## 5 CONCLUSIONS

In summary, it is reasonable to state that electrostatic energy and van der Waals energy were two major forces driving formation of the CpomPBP2–Dod complex. Attempts to disrupt these interactions, the electrostatic interaction in particular, decreased the binding affinity between CpomPBP2 and Dod. As dominant donors of electrostatic interactions, Glu98 and Arg109 were confirmed as two key residues determining the binding of Dod to CpomPBP2 protein. Not only that, energies unfavorable to the binding of Dod were also noted, including the unfavorable polar solvation energy derived from Glu98 and unfavorable electrostatic energy provided by Leu68. Such negative interactions provide cautions for the prospective chemical optimization of Dod. As an ingredient of *C. pomonella* sex pheromone, Dod works to synergize the effect of codlemone in attracting male moths, our results on the interaction between Dod and CpomPBP2 protein could boost the design and discovery of novel chemicals with similar functions.

### SUPPORTING INFORMATION

Prototype of the CpomPBP2–Dod complex (Fig. S1); Cluster analysis of the CpomPBP2–Dod complex produced in MD simulations (Fig. S2); Superimposition of representative conformations derived from dominant clusters (Fig. S3); The distances from atoms on the backbone of Dod to the closest residue atoms (Fig. S4); SDS–PAGE analysis of purified wild-type and mutant CpomPBP2 proteins (Fig. S5); Binding curves of 1–NPN to wild-type and mutant CpomPBP2 proteins (Fig. S6); Primers used for protein expression and site-directed mutagenesis (Table S1); Cluster analysis of the CpomPBP2–Dod complex based on the MD simulations trajectories (Table S2).

## ACKNOWLEDGEMENTS

This research was supported by the National Natural Science Foundation of China (31801797), the Natural Science Foundation of Jiangsu Province (BK20180902), the Key Research & Development Project of Shaanxi Province (2019NY-186), the Fundamental Research Funds for the Central Universities (2452018008), and the Sci-Tech Planning Project of Yangling Demonstration Zone (2018NY-02).

## SUPPORTING INFORMATION

Supporting information may be found in the online version of this article.

## REFERENCES

- 1 Beers EH, Suckling DM, Prokopy RJ and Avilla J, Ecology and management of apple arthropod pests. Ferree DC *Apples: Botany, Production and Uses*. CABI Publishing, Wallingford, pp. 489–519 (2003).
- 2 Witzgall P, Stelinski L, Gut L and Thomson D, Codling moth management and chemical ecology. *Annu Rev Entomol*; **53**: 503–522 (2008).
- 3 Coracini M, Bengtsson M, Liblikas I and Witzgall P, Attraction of codling moth males to apple volatiles. *Entomol Exp Appl*; **110**(1): 1–10 (2004).
- 4 Knight AL, Light DM, Judd GJ and Witzgall P. Pear ester – from discovery to delivery for improved codling moth management. J. Beck, SO. Duke, CC. Rering *Roles of Natural Products for Biorational Pesticides in Agriculture*. ACS Publications, Washington, DC pp. 83–113 (2018).
- 5 Light DM, Grant JA, Haff RP and Knight AL, Addition of pear ester with sex pheromone enhances disruption of mating by female codling moth (Lepidoptera: Tortricidae) in walnut orchards treated with meso dispensers. *Environ Entomol*; **46**(2): 319–327 (2017).
- 6 McGhee PS, Miller JR, Thomson DR and Gut LJ, Optimizing aerosol dispensers for mating disruption of codling moth, *Cydia pomonella* L. *J Chem Ecol*; **42**(7): 612–616 (2016).
- 7 Charmillot PJ, Hofer D and Pasquier D, Attract and kill: a new method for control of the codling moth *Cydia pomonella*. *Entomol Exp Appl*; **94**(2): 211–216 (2000).
- 8 Sumedrea M, Marin FC, Calinescu M, Sumedrea D and Iorgu A, Researches regarding the use of mating disruption pheromones in control of apple codling moth–*Cydia pomonella* L. *Agric Agric Sci Procedia*; **6**: 171–178 (2015).
- 9 Kydonieus AF, Beroza M, Zweig G, *Insect Suppression With Controlled Release Pheromone Systems*. CRC Press, Boca Raton, FL **1** (2017).
- 10 El-Sayed A, Suckling D, Byers J, Jang E and Wearing C, Potential of “lure and kill” in long-term pest management and eradication of invasive species. *J Econ Entomol*; **102**(3): 815–835 (2009).
- 11 Gut LJ and Brunner JF, Pheromone-based management of codling moth (Lepidoptera: Tortricidae) in Washington apple orchards. *J Agric Entomol*; **15**(4): 387–405 (1998).
- 12 Roelofs W, Comeau A, Hill A and Milicevic G, Sex attractant of the codling moth: characterization with electroantennogram technique. *Science*; **174**(4006): 297–299 (1971).
- 13 Arn H, Guerin P, Buser H, Rauscher S and Mani E, Sex pheromone blend of the codling moth, *Cydia pomonella*: evidence for a behavioral role of dodecan-1-ol. *Experientia*; **41**(11): 1482–1484 (1985).
- 14 McDonough L, Davis H, Chapman P and Smithhisler C, Response of male codling moths (*Cydia pomonella*) to components of conspecific female sex pheromone glands in flight tunnel tests. *J Chem Ecol*; **19**(8): 1737–1748 (1993).
- 15 Light DM, Control and monitoring of codling moth (Lepidoptera: Tortricidae) in walnut orchards treated with novel high-load, low-density “meso” dispensers of sex pheromone and pear ester. *Environ Entomol*; **45**(3): 700–707 (2016).
- 16 Knight A, Evaluating pheromone emission rate and blend in disrupting sexual communication of codling moth (Lepidoptera: Tortricidae). *Environ Entomol*; **24**(6): 1396–1403 (1995).
- 17 Wicher D. Olfactory signaling in insects. Teplow D *Progress in Molecular Biology and Translational Science*. Elsevier, pp. 37–54 (2015).
- 18 Elgar MA, Zhang D, Wang Q, Wittwer B, Pham HT, Johnson TL, Freelance CB and Coquilleau M, Focus: ecology and evolution: insect antennal morphology: the evolution of diverse solutions to odorant perception. *Yale J Biol Med*; **91**(4): 457 (2018).
- 19 Brito NF, Moreira MF and Melo AC, A look inside odorant-binding proteins in insect chemoreception. *J Insect Physiol*; **95**: 51–65 (2016).
- 20 Venthur H and Zhou J, Odorant receptors and odorant-binding proteins as insect pest control targets: a comparative analysis. *Front Physiol*; **9**: 1163 (2018).
- 21 Tian Z, Liu J and Zhang Y, Structural insights into *Cydia pomonella* pheromone binding protein 2 mediated prediction of potentially active semiochemicals. *Sci Rep*; **6**: 22336 (2016).

- 22 Tian Z and Zhang Y, Molecular characterization and functional analysis of pheromone binding protein 1 from *Cydia pomonella* (L.). *Insect Mol Biol*; **25**(6): 769–777 (2016).
- 23 Case D, Darden T, Cheatham T, III; Simmerling C, Wang, J, Duke, R, Walker R, Zhang W, Merz K, AMBER 12. University of California: San Francisco, CA (2012).
- 24 Liu J, Li Y, Tian Z, Sun H, Chen X, Zheng S and Zhang Y, Identification of key residues associated with the interaction between *Plutella xylostella* sigma-class glutathione S-transferase and the inhibitor S-hexyl glutathione. *J Agric Food Chem*; **66**(39): 10169–10178 (2018).
- 25 Jorgensen WL, Theoretical studies of medium effects on conformational equilibria. *J Phys Chem*; **87**(26): 5304–5314 (1983).
- 26 Tian Z, Li Y, Xing Y, Li R and Liu J, Structural insights into two representative conformations of the complex formed by *Grapholita molesta* (Busck) pheromone binding protein 2 and Z-8-dodecenyl acetate. *J Agric Food Chem*; **67**(16): 4425–4434 (2019).
- 27 Wang J, Wolf RM, Caldwell JW, Kollman PA and Case DA, Development and testing of a general amber force field. *J Comput Chem*; **25**(9): 1157–1174 (2004).
- 28 Jakalian A, Jack DB and Bayly CI, Fast, efficient generation of high-quality atomic charges. AM1-BCC model: II. Parameterization and validation. *J Comput Chem*; **23**(16): 1623–1641 (2002).
- 29 Hummer G, Rasaiah JC and Noworyta JP, Water conduction through the hydrophobic channel of a carbon nanotube. *Nature*; **414** (6860): 188–190 (2001).
- 30 Berendsen HJ, Postma JV, van Gunsteren WF, Di Nola A and Haak J, Molecular dynamics with coupling to an external bath. *J Chem Phys*; **81**(8): 3684–3690 (1984).
- 31 Hou T, Wang J, Li Y and Wang W, Assessing the performance of the molecular mechanics/Poisson Boltzmann surface area and molecular mechanics/generalized Born surface area methods. II. The accuracy of ranking poses generated from docking. *J Comput Chem*; **32** (5): 866–877 (2011).
- 32 Tian Z, Liu J and Zhang Y, Key residues involved in the interaction between *Cydia pomonella* pheromone binding protein 1 (CpomPBP1) and codlemone. *J Agric Food Chem*; **64**(42): 7994–8001 (2016).
- 33 Wang E, Sun H, Wang J, Wang Z, Liu H, Zhang J, Hou T, End-point binding free energy calculation with MM/PBSA and MM/GBSA: strategies and applications in drug design. *Chem Rev*; **119**: 9478–9508 (2019).
- 34 Weng G, Wang E, Chen F, Sun H, Wang Z, Hou T, Assessing the performance of MM/PBSA and MM/GBSA methods. 9. Prediction reliability of binding affinities and binding poses for protein-peptide complexes. *Phys Chem Chem Phys*; **21**: 10135–10145 (2019).
- 35 Weng G, Wang E, Wang Z, Liu H, Zhu F, Li D, Hou T, HawkDock: a web server to predict and analyze the protein–protein complex based on computational docking and MM/GBSA. *Nucleic Acids Res*; **47**: W322–W330 (2019).
- 36 Hou T, Wang J, Li Y and Wang W, Assessing the performance of the MM/PBSA and MM/GBSA methods. I. The accuracy of binding free energy calculations based on molecular dynamics simulations. *J Chem Inf Model*; **51**(1): 69–82 (2011).
- 37 Wang C, Greene DA, Xiao L, Qi R and Luo R, Recent developments and applications of the MMPBSA method. *Front Mol Biosci*; **4**: 87 (2018).
- 38 Metz A, Pflieger C, Kopitz H, Pfeiffer-Marek S, Baringhaus KH and Gohlke H, Hot spots and transient pockets: predicting the determinants of small-molecule binding to a protein–protein interface. *J Chem Inf Model*; **52**(1): 120–133 (2011).
- 39 Gohlke H, Kiel C and Case DA, Insights into protein–protein binding by binding free energy calculation and free energy decomposition for the Ras–Raf and Ras–RalGDS complexes. *J Mol Biol*; **330**(4): 891–913 (2003).
- 40 Raha K, van der Vaart AJ, Riley KE, Peters MB, Westerhoff LM, Kim H and Merz KM, Pairwise decomposition of residue interaction energies using semiempirical quantum mechanical methods in studies of protein–ligand interaction. *J Am Chem Soc*; **127**(18): 6583–6594 (2005).
- 41 Kollman PA, Massova I, Reyes C, Kuhn B, Huo S, Chong L, Lee M, Lee T, Duan Y and Wang W, Calculating structures and free energies of complex molecules: combining molecular mechanics and continuum models. *Acc Chem Res*; **33**(12): 889–897 (2000).
- 42 Miller III BR, McGee Jr TD, Swails JM, Homeyer N, Gohlke H and Roitberg AE, MMPBSA.py: an efficient program for end-state free energy calculations. *J Chem Theory*; **8**(9): 3314–3321 (2012).
- 43 Liu J, Tian Z, Zhou N, Liu X, Liao C, Lei B, Li J, Zhang S and Chen H, Targeting the apoptotic Mcl-1–PUMA interface with a dual-acting compound. *Oncotarget*; **8**(33): 54236 (2017), 54242.
- 44 Liu J, Tian Z and Zhang Y, Structure-based discovery of potentially active semiochemicals for *Cydia pomonella* (L.). *Sci Rep*; **6**: 34600 (2016).
- 45 Xu L, Sun H, Li Y, Wang J and Hou T, Assessing the performance of MM/PBSA and MM/GBSA methods. III. The impact of force fields and ligand charge models. *J Phys Chem B*; **117**(28): 8408–8421 (2013).
- 46 Sun H, Li Y, Tian S, Xu L and Hou T, Assessing the performance of MM/PBSA and MM/GBSA methods. IV. Accuracies of MM/PBSA and MM/GBSA methodologies evaluated by various simulation protocols using PDBbind data set. *Phys Chem* **16**(31): 16719–16729 (2014).
- 47 Moreira IS, Fernandes PA and Ramos MJ, Computational alanine scanning mutagenesis—an improved methodological approach. *J Comput Chem*; **28**(3): 644–654 (2007).
- 48 Cui G and Zhu J, Pheromone-based pest management in China: past, present, and future prospects. *J Chem Ecol*; **42**(7): 557–570 (2016).
- 49 Lu P, Huang L, Wang C, Semiochemicals used in chemical communication in the oriental fruit moth, *Grapholita molesta* Busck (Lepidoptera: Tortricidae). *Acta Entomol Sin*; **53**(12): 1390–1403 (2010).
- 50 Yang Z, Bengtsson M, Witzgall P, Host plant volatiles synergize response to sex pheromone in codling moth, *Cydia pomonella*. *J Chem Ecol*; **30**(2): 619–629 (2004).
- 51 Sandler BH, Nikonova L, Leal WS and Clardy J, Sexual attraction in the silkworm moth: structure of the pheromone-binding-protein–bombykol complex. *Chem Biol*; **7**(2): 143–151 (2000).
- 52 Lartigue A, Gruez A, Spinelli S, Rivière S, Brossut R, Tegoni M and Cambillau C, The crystal structure of a cockroach pheromone-binding protein suggests a new ligand binding and release mechanism. *J Biol Chem*; **278**(32): 30213–30218 (2003).
- 53 Shen J, Hu L, Dai J, Chen B, Zhong G and Zhou X, Mutations in pheromone-binding protein 3 contribute to pheromone response variations in *Plutella xylostella* (L.) (Lepidoptera: Plutellidae). *Pest Manag Sci*; **75**(7): 2034–2042 (2019).
- 54 Liu R, Lyu X, Batt S, Hsu M, Harbut M, Vilchère C, Cheng B, Ajayi K, Yang B, Yang Y, Guo H, Lin C, Gan F, Wang C, Franzblau S, Jacobs W, Besra G, Johnson E, Petrassi M, Chatterjee A, Fütterer K, Wang F, Determinants of the inhibition of DprE1 and CYP2C9 by antitubercular thiophenes. *Angew Chem Int Ed Engl*; **56**: 13011–13015 (2017).